

INTERACTION OF PARTICLES AND A MOVING ICE–LIQUID INTERFACE

Ch. KÖRBER and G. RAU

Helmholtz-Institut für Biomedizinische Technik an der RWTH Aachen, Pauwelsstrasse, D-5100 Aachen, Fed. Rep. of Germany

and

M.D. COSMAN and E.G. CRAVALHO

Harvard–MIT Division of Health Sciences and Technology, Cambridge, Massachusetts 02139, USA

Received 12 October 1984; manuscript received in final form 4 March 1985

A cryomicroscope was used to determine critical interface velocities marking the transition between repulsion and entrapment of spherical latex particles by an advancing ice–liquid interface. The employed freezing stage yields a planar ice front which propagates with increasing velocity into a region of decreasing thermal gradients. It was found that the critical velocity associated with the transition is inversely proportional to the particle radius as suggested theoretically under the assumption of the flat front (no cusping behind the particle). The critical velocity increases about linearly with the imposed thermal gradient which seems to stabilize the front against the perturbation induced by the particle. On the other hand, concentration gradients did not show a major effect: the addition of solute (0.56 mol% NaMnO₄) did not result in a significant change of the transition points as compared to the results obtained in pure water.

1. Introduction

The interaction of a macroscopic second-phase particle with a moving solidification front can lead to its encapsulation or rejection, i.e., the particle either remains stationary and becomes entrapped by the advancing interface, or it is being pushed and swept along with the solidification front. The phenomenon is of crucial importance for many applications in metallurgy, materials science and crystal growing. It is either necessary to purify the solid phase and to keep it free of second-phase inclusions, or it may be desirable to achieve a controlled incorporation of (e.g. ceramic) particles yielding better mechanical or electrical properties of the solid matrix. Relating to that background, many studies have been carried out in the past few decades and have eventually lead to a more detailed understanding of the underlying principles and mechanisms.

More recently it has also been recognized, that the phenomenon plays a significant role for the

cryopreservation of biological cell suspensions [1,2]. The freezing of aqueous salt solutions (which are commonly used as a suspension medium) may result in considerable deviations from equilibrium as given by the respective phase diagram. It was observed that solute rejection can lead to large concentration gradients in the residual liquid with the solute becoming highly enriched immediately ahead of the advancing ice–liquid interface [3]. As most biological cells are damaged osmotically when subjected to salt concentrations above a critical limit [4,5] it is obvious that detrimental effects are to be expected when the cell is being pushed by the ice front and thus becomes exposed to increasing salt concentrations for an extended period of time. Conditions resulting in a repulsion of the cell should hence be clearly avoided when designing a successful cryopreservation procedure. As suggested by Brower and coworkers [2], it may be desirable to get the cells encapsulated immediately upon arrival of a (plane) ice front, thus circumventing the exposure to high salt concentra-

tions that would develop ahead of the front during "pushing" or in the channels of residual liquid during non-planar freezing. Unfortunately, there is only very little evidence on the interaction of biological cells with a moving ice-liquid interface and it is generally not possible to predict the conditions under which encapsulation or rejection takes place.

In contrast to biological cells, the behavior of organic and inorganic particles of various shapes, phases, dimensions, and surface properties has been studied in a number of different matrices [6-9] including ice [10,11]. A critical review of the reported data may be found in ref. [12]. However, it has not yet been investigated in systematic experiments to what extent the variation of thermal gradients or the addition of solutes affects the results. From theoretical analyses [11-16] it can be expected that these parameters play a significant role, particularly in situations relating to the freezing of biological cell suspensions where varying gradients of temperature and solute concentration are encountered. Hence it was felt to be necessary to determine how the behavior of solid particles is influenced by these effects before investigating biological cells exposed to similar conditions. In this contribution, we present results obtained with solid particles to elucidate the more fundamental aspects. Observations with yeast cells which were used as a biological model system will be reported in a separate paper [36].

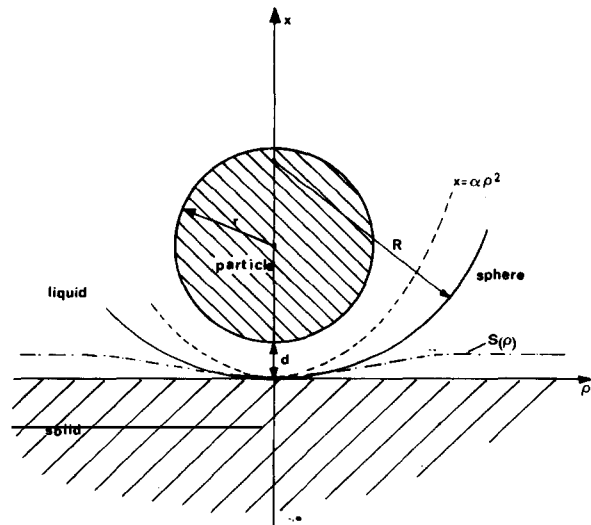
2. Theoretical background

A particle being pushed ahead of an advancing solid-liquid interface is subject to two counteracting forces, an attractive one resulting from viscous drag due to fluid flow around the particle which favors entrapment, and a repulsive one which originates from Van der Waals forces and may be expressed in terms of differences in interfacial free energy. Under steady state conditions and when no external forces are involved the sum of the forces acting on the particle must be zero. During pushing, the particle cannot directly touch the phase boundary: a film of liquid of a sufficient thickness must exist in between in order to main-

tain the transport of molecules towards the growing crystal surface behind the particle. With increasing velocity of the solidification front, the distance between particle and phase boundary becomes smaller while both forces increase. If a critical velocity is reached, the forces cannot be balanced any more and the distance of the gap is no longer sufficient to keep the crystal surface growing. As a result the particle becomes encapsulated.

In a number of approaches, the involved forces and the resulting critical interface velocities have been determined for various sets of conditions and assumptions [9,12-21]. A good survey of the respective literature up to 1978 was presented by Aubourg [12]. In the following, we will therefore just give a brief outline of the underlying principles and discuss the results relating to the case considered here.

Fig. 1 sketches a situation where a smooth, spherical, and rigid particle of radius r is moving a distance $d \ll r$ ahead of a solid-liquid interface advancing with velocity v . Under steady state conditions, the attractive and disjoining forces can be determined as follows.



Sketch of a spherical particle of radius r being swept a distance d ahead of a solid-liquid interface $S(\rho)$ advancing with velocity v .

2.1. Attractive drag force

For a particle moving very close to a solidification front, the standard Stokes' equation for the drag force is no longer valid as the flow of liquid is perturbed by the front. Carrier [22] has derived the following expression for the case of a flat interface

$$F_{\eta} = 6\pi\eta vr^2/d, \quad (1)$$

where η denotes the viscosity of the liquid suspension medium (see also the list of symbols at the end).

2.2. Disjoining force

Thermodynamic arguments show that a particle can only be rejected if the interfacial free energy between the particle and the solid phase, σ_{sp} , is larger than the sum of the surface free energies solid-liquid, σ_{sl} , and liquid-particle, σ_{lp} :

$$\Delta\sigma_0 = \sigma_{sp} - (\sigma_{sl} + \sigma_{lp}) > 0. \quad (2)$$

Otherwise, a state of lowest energy is achieved when the particle is completely surrounded by solid. For the case of a spherical particle of radius r in direct contact with the solidification front, the corresponding repulsive force can be derived as [20,21]

$$F_{\sigma} = 2\pi r \Delta\sigma_0. \quad (3)$$

For a thin film of liquid between particle and front, this expression has to be modified. Uhlmann et al. [9] suggested that the surface energy of a thin layer of liquid is a function of the thickness of the film, replacing eq. (3) by

$$F_{\sigma} = 2\pi r \Delta\sigma_0 (a_0/d)^n, \quad (4)$$

where a_0 is the average intermolecular distance in the film and the exponent n used in ref. [9] ranged from 4 to 5. The form of the relationship given in (4) agrees with the disjoining term due to Van der Waals forces if the involved Hamaker constants are determined appropriately [12,20,21]. However, Aubourg [12] and Chernov et al. [18] derived $n = 2$ for small d and $n = 3$ for larger d , while Pötschke [21] and Langbein [16] used values between 1 and 4.

From the balance of both forces, i.e. putting $F_{\eta} = F_{\sigma}$ as in eqs. (1) and (4), one obtains the critical velocity v_c marking the transition from particle rejection to encapsulation (cf. also refs. [9,20]):

$$v_c = \frac{\Delta\sigma_0 d}{3\eta r} \left(\frac{a_0}{d} \right)^n. \quad (5)$$

For a flat solidification front, the critical velocity should hence be inversely proportional to the particle radius. The main problem associated with eq. (5) is the determination of correct values for d and n and the uncertainty of experimental values for $\Delta\sigma_0$. The proportionality coefficient in (5) can therefore in general only be roughly estimated for most practical situations.

Several authors have refined the treatment of the problem by considering different geometries of the interface as well as the particle and by including effects due to heat conduction and solute diffusion.

2.3. Different geometries

For a disc in front of a flat interface, Aubourg [12] showed that the critical velocity varies with r^{-3} instead of r^{-1} . Uhlmann et al. [9] treated the case of irregularities on the surface of a spherical particle which reduce the effective radius and can hence lead to critical velocities considerably higher than for comparable smooth particles. If the interface is non-planar, it is clear that the contour of the front must be of radial symmetry with respect to the particle. In the simplest case of a front concentric to a spherical particle [12], the expression for the critical velocity, eq. (5), has to be corrected by a factor depending on the radius of the dimpled area. If the front is not concentric to the particle, the width of the gap is no longer constant yielding a more complicated correction factor [12,17,21]. For a slightly curved interface this factor reduces to $(1 - r/R)$ where R is the radius of curvature. Chernov and coworkers [18] have assumed a parabolical shape of the front and received $v_c \sim r^{-4/3}$ for small particles ($r \leq 500 \mu\text{m}$). A general expression for a spherical particle ahead of an interface of arbitrary given contour

$S(\rho)$ was derived by Bolling and Cissé [17]. Evaluated for the limiting case of maximum drag force, this yields $v_c \sim r^{-3/2}$. They also considered the situation of a particle pushed ahead of a grain boundary groove, resulting in an increase of v_c by a factor of $\sqrt{2}$ or $\sqrt{3}$ (triple point).

The various expressions for a smooth spherical particle and solidification fronts of different geometries can be summarized by expressing them in the form

$$v_c = k' \frac{1}{\eta} \frac{1}{r^m}, \quad (6)$$

where the exponent m varies between 1 and 3/2 and k' is a proportionality factor that depends on geometry and the difference of surface free energy, $\Delta\sigma_0$. It should be noted that cusping of the front behind the particle increases the drag force more than the disjoining force, and that the value of the critical velocity can hence be drastically reduced as compared to the case of a flat interface (eq. (5)).

2.4. Thermal effects

The shape of the solidification front behind the front is obviously affected by the temperature distribution in the particle-matrix system. It can hence be expected that the critical velocity also depends on the thermal conditions applied to the sample. For a (constant) temperature gradient $G = dT/dx$ imposed on the matrix, Hoekstra and Miller [11] found a relationship similar to eq. (6) but indicating a linear increase of v_c with G :

$$v_c = k'' \frac{d}{\eta} \frac{1}{r} G. \quad (7)$$

According to a different approach by Chernov and coworkers [18], however, this dependence is compensated by the Gibbs-Thomson effect for small particles ($r \leq 500 \mu\text{m}$). For larger particles, they derived that v_c varies as $G^{1/4}$. However, a re-evaluation of their calculations by Pötschke [21] showed that the influence of the thermal gradient cancels out completely for pure systems. In a subsequent paper [14], Chernov et al. also considered the effect of different thermal conductivities of particle and matrix, λ_p and λ_m , respectively. As already suggested qualitatively in ref. [17], it

was shown that the front dimples and becomes concave behind the particle if $\lambda_p > \lambda_m$, resulting in a reduction of the critical velocity, while the front is raised and v_c increased for the opposite case of $\lambda_p < \lambda_m$ (which particularly applies to the entrapment of gas bubbles). Aubourg [12] and Langbein [16] have presented numerical determinations of the shape of the solidification front for different thermal conductivities.

2.5. Solute effects

Temkin et al. [15] have neglected the influence of thermal gradients and took into account the diffusion of dissolved impurities in their determination of the critical velocity. For particles of small diameter with respect to the thickness of the diffusion boundary layer, they assumed steady state conditions and balanced hydrodynamic and diffusion flow in a cylindrical area behind the particle. Their results suggest an enrichment of solute in the gap between particle and interface, leading to a concave shape of the front due to the resulting reduction of the melting point. Accordingly, the critical velocity should be lower than for pure substances and vary with r^{-2} instead of $r^{-4/3}$. Chernov and Bronstein [13] have considered an electrostatic contribution to the disjoining force resulting from the interaction of the contact potential between particle and matrix and the potential due to differential adsorption and incorporation of anions and cations at the interface ("freezing potential", "Workman-Reynolds Effect" [23,24]). Their calculations for dilute solutions yield $v_c \sim r^{-1}$ for small particles and $v_c \sim r^{-2}$ for large particles where the limiting radius depends on the contact potential and the impurity concentration at the interface. It is not well established, however, what values have to be used for the involved potentials. Moreover, the steady state conditions assumed in both papers [13,15] are generally not encountered in aqueous systems with extremely small distribution coefficients k [25].

In conclusion, it may be stated that the basic mechanisms controlling the rejection or entrapment of particles by a solidification front in steady-state have been recognized and described appropriately. However, the applicability of the re-

sults to practical situations is difficult as the magnitude of some of the involved quantities is rather uncertain. The understanding of the influence of thermal and solute effects and their combination is still incomplete and limited by a number of rough approximations.

3. Materials and methods

A means to study the interaction of particles and an advancing ice front was apparent in a set-up which was previously used to determine concentration profiles due to solute rejection and the transition from a flat interface to non-planar morphologies during the freezing of electrolyte solutions [3,26,27]. This offers the advantage that the time and space dependent distributions of temperature and solute concentration in the sample are well established. The arrangement basically consists of a cryomicroscope [28,29] equipped with a special freezing stage [3] which yields a precisely controlled propagation and shape of the ice-liquid interface in combination with simultaneous visual observation and/or video-recording for subsequent quantitative evaluation. The main difference as compared to other approaches in determining critical interface velocities is that the thermal gradient at the front and its velocity are not being kept constant, but decrease and increase, respectively, during the course of the experiment. The arrangement is hence more similar to the solidification process as it occurs in practical freezing situations where the ice fronts propagate from an area of high temperature gradients close to the cold walls of a freezing container towards a point of vanishing thermal gradient in the center of the system [30]. As outlined below, it also offers the advantage of determining the critical interface velocity and the corresponding temperature gradient in a single run.

The sample suspension is put on the freezing stage as a thin layer (about 20 μm thick) between two glass surfaces. The temperature profile imposed on this sandwich-like arrangement produces two parallel ice fronts advancing from the edges of the observation slit toward its center where they eventually meet. From a simple model described

elsewhere [3,27] one can derive a parabolical temperature profile across the slit, which is lowered linearly with time by imposing a constant cooling rate B at the center (where the thermocouple junction providing the input signal to the thermal control system is positioned). Under quasi-stationary conditions, i.e. sufficiently slow cooling, one obtains

$$T(x, t) = T_0 + Bt - \frac{1}{\gamma^2} (T_0 + Bt - T_{\text{Cu}}) (x_{\text{R}} - x)^2, \quad (8)$$

where T_0 is the starting temperature, T_{Cu} the temperature of the copper substage, x_{R} the half-width of the (symmetrical) system and γ^2 a factor related to the heat transfer coefficient between the copper block and the glass sheet supporting the sample layer. The time dependence of the 0°C isotherm, i.e. the position of the ice front (assuming equilibrium at the interface) then becomes

$$\xi(t) = x_{\text{R}} - \gamma \left(1 - \frac{T_{\text{Cu}}}{T_0 + Bt} \right)^{-1/2} \quad (9)$$

From this, one can derive the position dependence of the interface velocity

$$v(\xi) = \frac{\bar{B} [(x_{\text{R}} - \xi)^2 - \gamma^2]^2}{2\gamma^2 T_{\text{Cu}} (x_{\text{R}} - \xi)}, \quad (10)$$

and the position dependence of the thermal gradient at the interface

$$G(\xi) = \left. \frac{\partial T}{\partial x} \right|_{\xi} = \frac{2(x_{\text{R}} - \xi) T_{\text{Cu}}}{(x_{\text{R}} - \xi)^2 - \gamma^2}, \quad (11)$$

which is independent from the imposed cooling rate B . Fig. 2 gives a graphical representation of eqs. (10) and (11) for typical set of values γ , T_{Cu} , x_{R} and various B . As mentioned above, one recognizes that the interface velocity continuously increases when the ice front approaches the center of the slit while the gradient decreases and eventually vanishes at that point. It can also be seen that for increasing cooling rates B , a certain value of the interface velocity is reached at decreasing values of ξ , i.e. closer to the edge of the slit and hence at higher thermal gradients. From the position at which a particle becomes encapsulated, one can

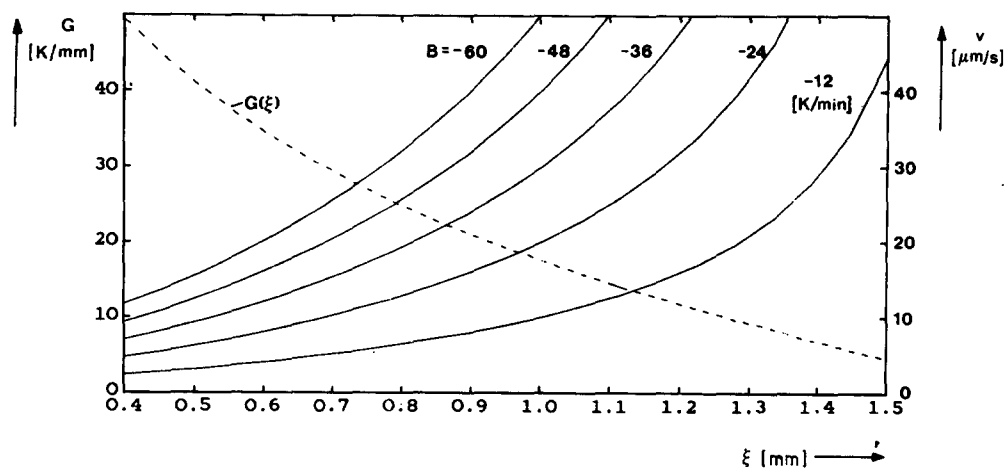


Fig. 2. Position dependence of interface velocity $v(\xi)$ and thermal gradient and interface, $G(\xi)$ according to eqs. (10) and (11), respectively. $T_{Cu} = -44^{\circ}\text{C}$, $x_R = 1.7$ mm, $\gamma = 2.0$ mm

thus determine the critical velocity and the corresponding gradient according to eqs. (10) and (11). The needed thermal parameters can be obtained by evaluating the interface propagation kinetics as given by eq. (19).

The suspension media used in this study were either distilled water or a binary aqueous solution of 0.56 mol% NaMnO_4 , which was previously studied [3,27] as a model substance with mass diffusive and phase diagram properties very similar to NaCl which is of main interest in cryobiological applications. It absorbs light in the visual range (maximum absorption at 525 nm) and can hence be used to visualize the concentration distribution in the sample solution layer and also allows quantitative photometric measurements. The particles used in this study were latex spheres of two different diameters, 5.7 ± 1.5 μm and 11.9 ± 1.9 μm (Sigma, St. Louis, MO 63178, USA. and Dow Chemical, Indianapolis, IN 46206, USA). The size distributions were checked under the microscope and found to be in satisfactory agreement with those stated by the supplier. The material, styrene divinylbenzene, has a density of 1.05 g/cm^3 which is sufficiently close to that of the matrix materials to avoid significant gravitational effects due to buoyancy. The presence of surfactants which could be left over from the production process of the latex spheres and which could possibly contaminate the sample suspension was checked by

means of the capillary rise method. No significant differences could be found compared to the pure suspension medium.

The concentration of particles in the suspension was adjusted according to two limiting criteria: on the one hand the concentration had to be low enough to avoid a pile-up of particles in front of the interface before the critical velocity was reached (in that case, the flow fields around the individual particles could interact and become disturbed). On the other hand, it was necessary to keep a sufficient number of particles (usually between 30 and 50) in the field of observation. A typical value of the resulting particle concentrations was approximately 2×10^4 mm^{-3} .

4. Results and discussion

Fig. 3 shows a sequence of photographs representing the various phases of the freezing process in the suspension (latex spheres of 5.7 μm mean diameter in distilled water). The pictures were taken in time intervals of about 30 s and show the same section within the left half of the observation slit as the ice front advances through the sample toward the center (from left to right) [31].

One can distinguish three different phases:

(1) All particles are being pushed as the ice front is still advancing rather slowly with a velocity below the critical value v_c .

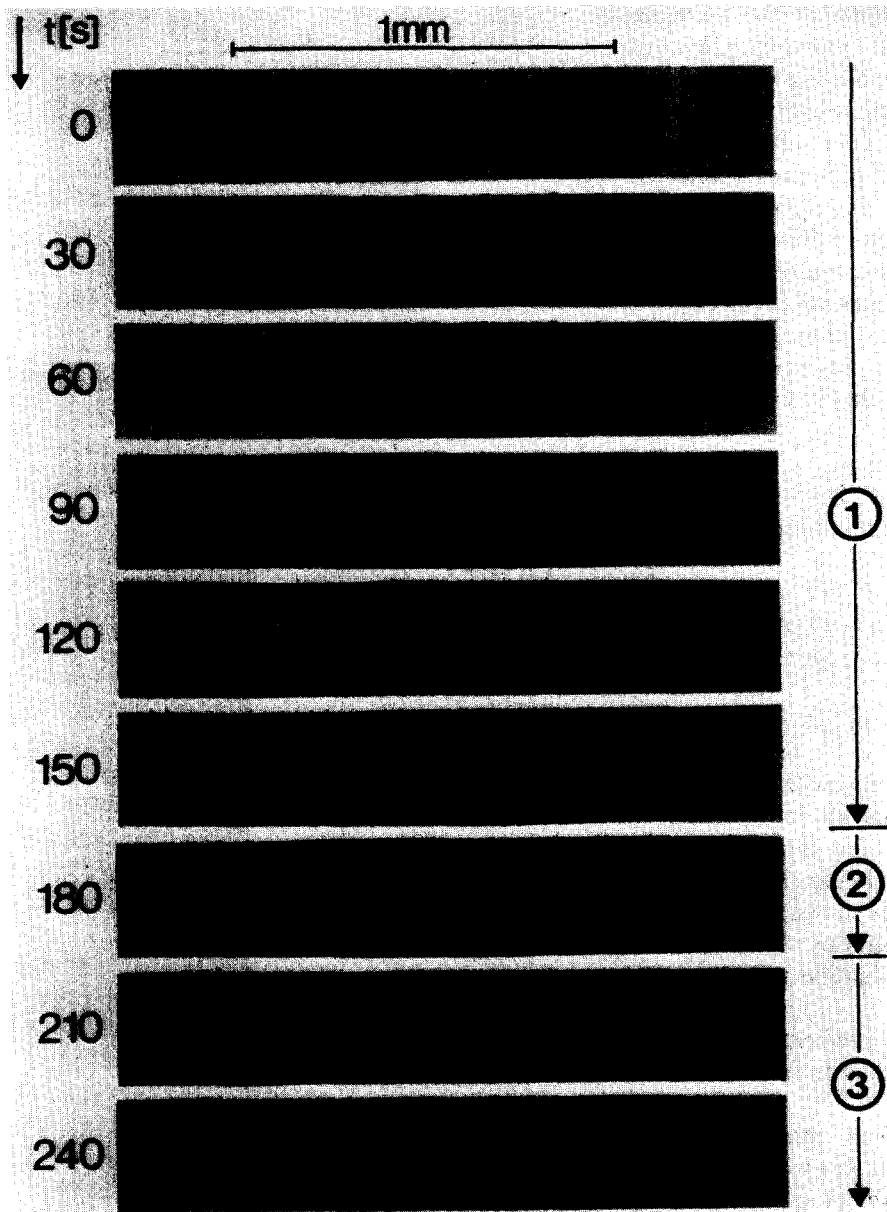


Fig. 3. Series of photographs showing a section of the observation slit as the ice-liquid interface passes through the suspension ($5.7 \mu\text{m}$ diameter latex spheres in water). Time interval $\Delta t = 30 \text{ s}$, cooling rate $B = -10 \text{ K/min}$, substage temperature $T_{Cu} = -60^\circ\text{C}$.

(2) The particles are gradually left behind as their critical velocities are reached. At this point, only two of the particles that were previously pushed are not yet encapsulated. Some particles are only swept along for a very short distance before they get entrapped.

(3) All particles remain in their initial position and are encapsulated immediately upon arrival of the ice front. The interface velocity is beyond the critical value v_c .

It can be seen that the ice front remained planar during the whole sequence of pictures shown

in fig. 3: dendritic breakdown of the interface occurred at a velocity well above v_c . This, of course, is a result of the stabilizing effect of the thermal gradients in the system, which are governed by the temperature of the copper substage (cf. eq. (11)). The value of T_{Cu} had hence to be selected low enough to maintain the interface planar and sufficiently stable against deformations within the range of positions where the transition between particle rejection and encapsulation occurred.

Fig. 4 shows a sequence of photographs where the camera frame was kept at rest with respect to the advancing interface. In this case the suspension medium was 0.56 mol% NaMnO_4 and the ice front was moving faster than in fig. 3 due to the larger imposed cooling rate ($B = -15 \text{ K/min}$). The transition from pushing to entrapment occurs between $\xi = 0.784 \text{ mm}$ (third frame from top) and $\xi = 0.900 \text{ mm}$ (sixth frame). It can also be recognized from the more intense blackening ahead of the front, that a diffusion boundary layer is built up due to the rejection of solute, which finally leads to dendritic breakdown (bottom frame $\xi = 1.024 \text{ mm}$). Under the conditions examined here, cell spacing, i.e. the average distance of the liquid channels between the tongue like protrusions, is almost an order of magnitude larger than the average particle diameter. It should also be pointed out that some of the particles shown in figs. 3 and 4 were entrapped under conditions which were not suitable for quantitative evaluation as will be explained below.

When determining critical velocities, a number of precautions had to be taken in order to avoid erroneous results:

- (1) Particles pushed ahead of grain boundary grooves were not evaluated as this would presumably result in higher critical velocities than pushing by a plane front (cf. ref. [17]).
- (2) Aggregations of two or more particles were not considered for the reasons outlined above.
- (3) Particles which adhered to the glass surface were excluded from evaluation.

Keeping these sources of possible error in mind, critical velocities were only determined for single particles in front of a plane interface which were swept along for a distance of at least five particle diameters before they were encapsulated. Instead

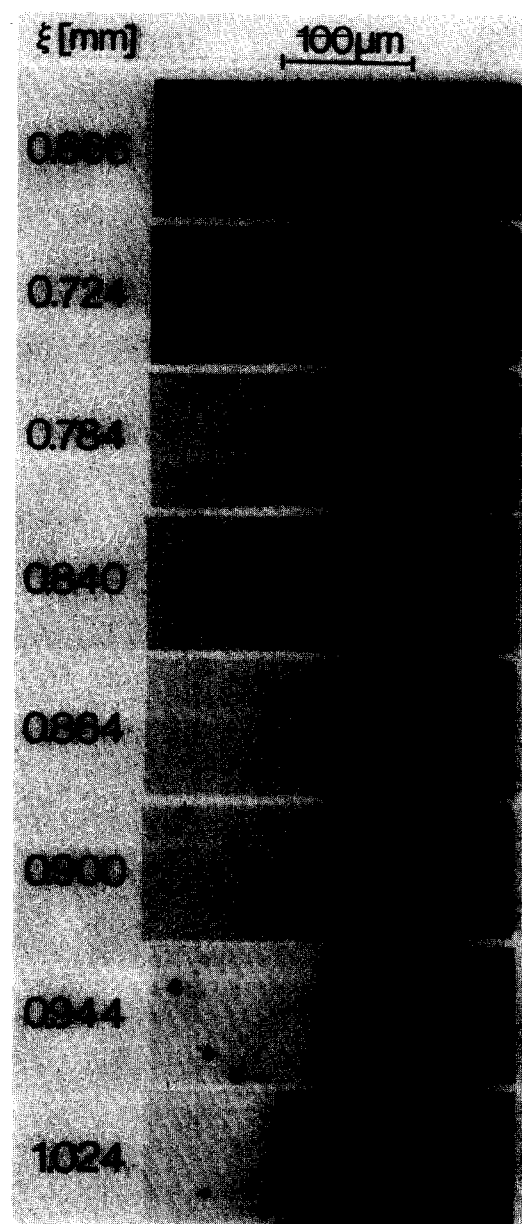


Fig. 4. Series of photographs taken at non-uniform time intervals with camera frame at rest with respect to the moving interface (positions ξ relative to the edge of the slit given at left). Latex spheres of $5.7 \mu\text{m}$ mean diameter suspended in 0.56 mol% NaMnO_4 . Cooling rate $B = -15 \text{ K/min}$, substage temperature $T_{Cu} = -60^\circ\text{C}$.

of using still pictures, the experiments were evaluated from video tape recordings because of the higher time resolution and the better possibili-

ties of keeping track of the individual particles.

The procedure used for evaluation will be briefly described by the following example. First, the propagation kinetics of the interface was determined by fitting a curve (least squares fit) according to eq. (9) to a set of about 10 to 15 position-time data points cf. fig. 5). Generally, between 5 and 10 iterations were needed to obtain a converging fit (criterion: relative improvement of better than 10^{-4} in the sum of squares from one iteration to the other). The multiple r^2 -values (ratio of regression and total sum of squares) were larger than 0.996 in all cases. Second, the positions at which encapsulation occurred according to the criteria given above were determined for about 30 to 50 particles. This yields a frequency distribution of transition points, an example of which is given in fig. 6 (results from same experiment as in fig. 5). The width of this distribution is mainly related to the particle size distribution but also reflects effects that are not precisely known like inhomogeneities of the particle surface or deviations from sphericity. A critical position \bar{x}_c and standard deviation was defined as the weighted mean value of this distribution ($\bar{x}_c = 1.085 \pm 0.096$ mm for the

case presented in figs. 5 and 6). Finally, the critical velocity, v_c , and the corresponding thermal gradient, G_c , were computed by solving eqs. (10) and (11), respectively, for \bar{x}_c and the set of parameters determined previously.

As the size distribution of the latex beads is rather broad, an attempt was also made to determine the effect of the particle diameter on the transition points. For this purpose, the distribution was subdivided into classes of equal size, and the mean value of the critical velocity was evaluated separately for each class. Fig. 7 shows the resulting plot of critical velocity (mean \pm standard deviation) versus particle radius. It becomes clear that the critical velocity decreases with increasing particle size as predicted by all theoretical models. For relating the data to the various functional relationships derived from those models, a least squares fit was performed according to eq. (6). Fig. 7 gives the curves obtained by adjusting the proportionality factor in eq. (6) for the different values of the exponent m , i.e. the solid curve for $m = 1$ [9,11], the dotted curve for $m = 4/3$ [18] and the dashed curve for $m = 3/2$ [17]. The best agreement with our experiments is achieved by

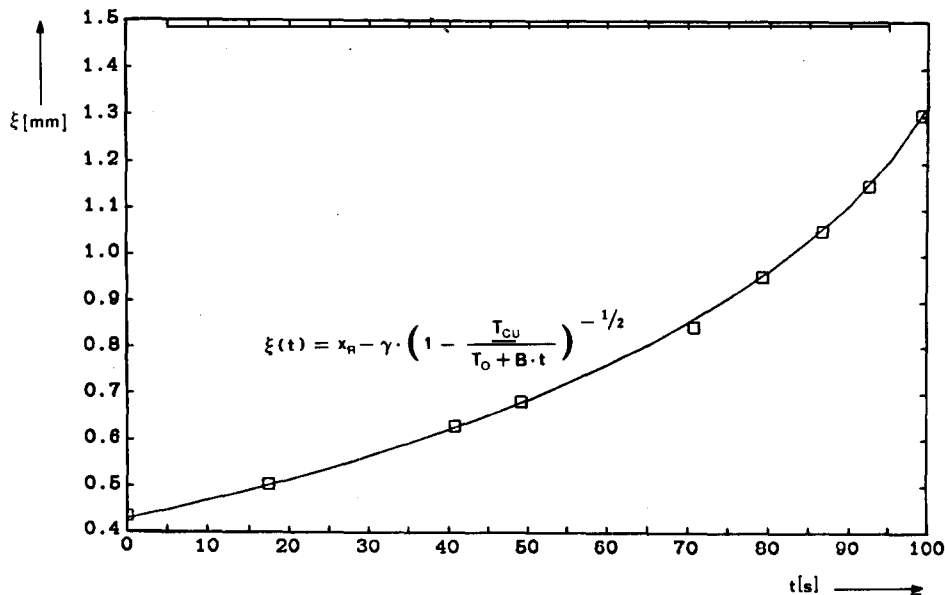


Fig. 5. Interface propagation kinetics for $T_{Cu} = -44^\circ\text{C}$ and $B = -0.246$ K/s (-14.8 K/min) with fitted curve ($T_0 = 26.46^\circ\text{C}$, $x_R = 1.76$ mm, $\gamma = 2.17$ mm).

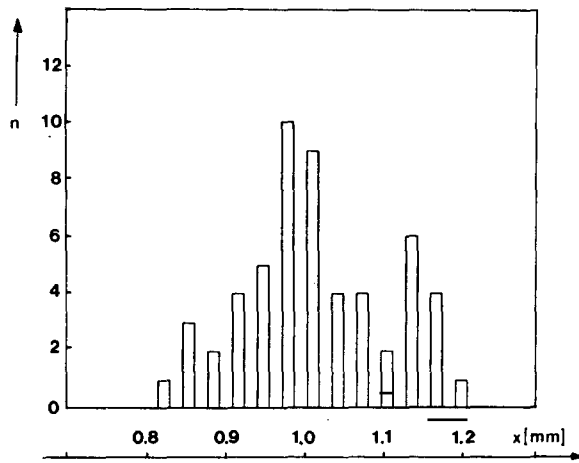


Fig. 6. Frequency distribution of transition points observed under conditions given in fig. 5 (n : number of particles; $\Delta x = 32.5 \mu\text{m}$ channel width). Critical positions $\bar{x}_c = 1.085 \pm 0.096 \text{ mm}$ (mean \pm standard deviation).

putting $m = 1$, resulting in $k'/\eta = 0.09397 \times 10^{-3} \text{ mm}^2/\text{s}$ (final sum of squares 0.11×10^{-3} , $r^2 = 0.9782$). This would imply that the assumption of the flat ice-liquid interface represents a reasonable approximation, allowing the rather simple treatment leading to eq. (5) as outlined above. In fact, a deformation of the front behind the particle could never be detected in our observations. It has to be noted, however, that the results have a

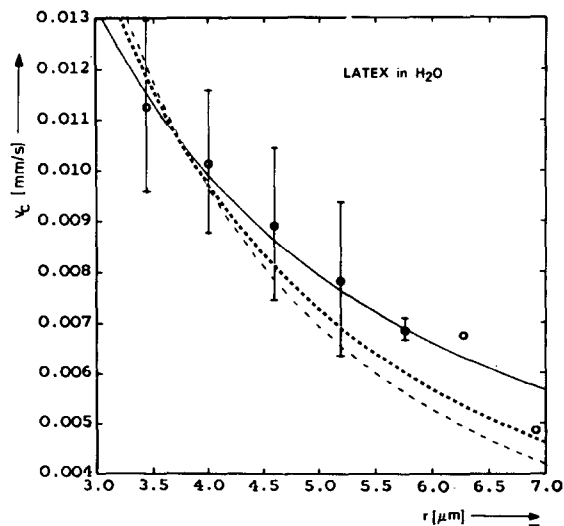


Fig. 7. Critical velocity v_c (\pm standard deviation) versus particle radius r . Solid line shows fitted function $v_c = 0.0397r^{-1}$, dotted line $v_c = 0.0621 r^{-4/3}$, dashed line $v_c = 0.0775r^{-3/2}$.

relatively large standard deviation and that the range of particle diameters investigated in this study is rather small, making extrapolations problematic.

Similar limitations have to be made when comparing the proportionality coefficient resulting from the fitted curve ($m = 1$) to that obtained theoretically in eq. (5) for a planar interface. In principle, it would be possible to determine the distance d between front and particle if the other parameters were precisely known. As mentioned above, however, further assumptions would have to be made with respect to the values of the exponent n and the difference of surface free energies, $\Delta\sigma_0$, which is not known for the material combination studied here. Further uncertainties could arise from the fact that the viscosity of very thin films may be considerably larger than that of the bulk liquid as discussed in ref. [18]. Taking $n = 2$ as proposed in ref. [12] and $\Delta\sigma_0 = 0.05 \text{ N/m}$ as suggested by Uhlmann [9], a rough estimate can be made for d . With the intermolecular distance in water, $a_0 = 3.8 \text{ \AA}$, and viscosity $\eta = 1.8 \text{ cP}$, one obtains $d = 335 \text{ \AA}$. With $n = 3$ and the same values, one gets $d = 112 \text{ \AA}$. The distance of the gap between particle and front should hence be filled by at least several tens of water molecules. This result is within the range of Langbein's [19] estimate that d varies between 10 and 1000 \AA (Bolling and Cissé proposed $d = 6a_0 = 23 \text{ \AA}$). Distances of this order of magnitude are clearly beyond the resolution limits of light microscopy, hence an independent measurement of d was not possible in this study. It should be stated, however, that in our observations the particles always appeared directly in touch with the interface, indicating that d is at least smaller than the resolution limit of the microscope.

The influence of solute effects on the transition from pushing to encapsulation was studied with latex beads of $5.7 \mu\text{m}$ diameter which were suspended either in distilled water or in 0.56 mol% NaMnO_4 solution. Fig. 8 shows the positions at which entrapment occurred for different cooling rates in both matrix media and otherwise identical conditions. Evidently, there is no significant difference, indicating that the amount of solute added does not play a major role in the interaction

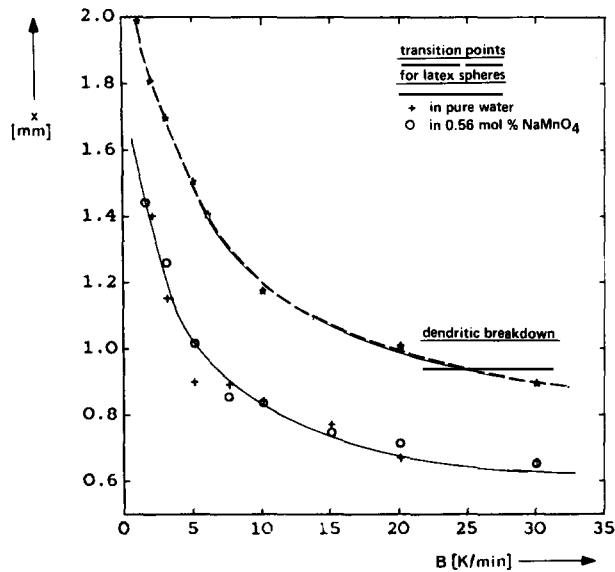


Fig. 8. Critical position marking the transition from particle rejection to entrapment in distilled water (+) and in 0.56 mol% NaMnO_4 (O) versus cooling rate B . Latex particles of $5.7 \mu\text{m}$ mean diameter, substage temperature $T_{\text{Cu}} = -60^\circ\text{C}$. Dashed curve (*) represents dendritic breakdown points.

of particles and icefront. Hence our results do not confirm the theoretical model proposed by Temkin and coworkers [15] who predicted an enrichment of impurity in the gap between particles and front, resulting in a concave deformation of the interface and thus a reduction of the critical velocity as compared to pure substances. The discrepancy might be due to two possible reasons: First, the distribution coefficient of electrolytes in ice is of the order of magnitude $k = 10^{-8} - 10^{-6}$ [25], i.e. impurities are almost completely rejected by the advancing ice front. That leads to a continuous increase of both the absolute solute content and the concentration gradient at the interface [3,32]. Steady state conditions as considered by Temkin et al. [15] are hence not encountered during planar freezing in electrolyte solutions, and solute enrichment can become extremely high. Second, Temkin and coworkers have not considered the additional effect of thermal gradients, which would counteract the deformation of the front due to the accumulation of impurity behind the particle. As our system, on the other hand, does exhibit rather strong temperature gradients (cf. figs. 2 and 9)

their influence on the critical velocity (which will be discussed below) might possibly conceal that of solute enrichment. Unfortunately, a theory taking into account the coupled effect of both heat and mass diffusion has not been developed so far to our knowledge. A comparison of our results with Chernov and Bronstein's model [13] considering an electrostatic component of the disjoining force is not possible as the amount of the involved potentials is not known. Although their model also predicts $v_c \sim r^{-1}$ for small particles, the proportionality coefficient depends strongly on the potentials and can therefore not be related to that of pure substances. Without knowing the values of the potentials it can hence not even be stated whether the presence of electrolytes should produce an increase or a reduction of the critical velocity.

Fig. 9 shows the relationship between critical velocity and thermal gradient at the interface for latex beads of $5.7 \mu\text{m}$ diameter suspended in pure water. Apparently, a steeper thermal profile requires a more rapid interface propagation for inducing the transition between pushing and en-

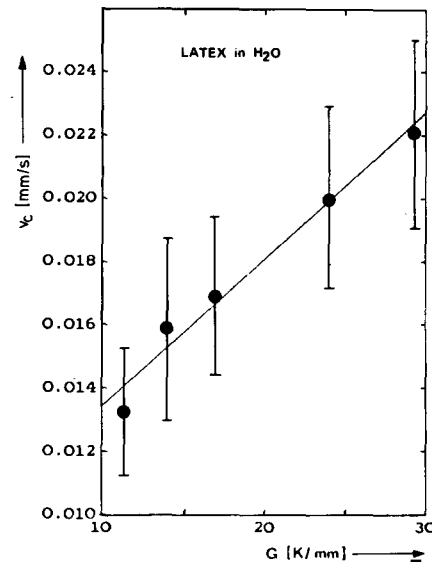


Fig. 9. Relationship between critical velocity v_c and thermal gradient at the interface for latex particles of $5.7 \mu\text{m}$ mean diameter in distilled water. Solid line represents least squares fit. Error bars show standard deviations.

capsulation. Such an increase of v_c with increasing thermal gradients in the matrix was also predicted by the models taking into account a non-uniform temperature distribution [11,14]. Our results indicate a linear relationship as proposed by Hoekstra and Miller according to eq. (7). However, the uncertainties relating to the assumptions in their derivation have to be kept in mind, and the limited range of the conditions investigated so far makes a definite statement difficult with respect to the functional dependency. It is conceivable that a constant value is reached asymptotically for very large gradients. Extrapolating to vanishing G , the linear regression line in fig. 9 yields $v_c(G=0) = 8.78 \mu\text{m/s}$, but it should be mentioned that the analysis of very small gradients would bring up experimental difficulties and might lead to different results.

It is clear, though, that thermal gradients have a stabilizing effect, possibly in a similar way as they do in constitutional supercooling and interface breakdown due to solute build-up ahead of the advancing solidification front in alloys and solutions [33–35]. Another qualitative resemblance might be derived from the shape of the dashed curve in fig. 8. It represents the transition points corresponding to dendritic breakdown, i.e. the positions at which the previously planar interface becomes morphologically unstable due to solute rejection and constitutional supercooling. It can be seen that the pushing-encapsulation transition always occurred before dendritic breakdown, and that both curves are of approximately the same shape. This might also suggest that similar mechanisms may be involved in both phenomena. The breakdown of a planar front due to solute rejection is generally understood in terms of interface stability theories considering the development of an arbitrary sinusoidal perturbation with respect to heat and mass diffusion and capillarity effects [33–35]. A more detailed understanding of particle rejection and encapsulation might hence be achieved by additionally incorporating the perturbations induced by the particle, i.e. combining the models describing the interaction due to viscous drag and surface effects with interface stability theories taking into account coupled heat and mass diffusion.

5. Conclusions and outlook

It was shown that a cryomicroscope system designed for the investigation of solute redistribution and interface instabilities also serves as a useful tool for determining the transition between particle repulsion and encapsulation by the advancing ice-liquid interface. The critical velocity can be determined in a single run as the motion of the interface is continuously accelerated. The transition observed for latex spheres in aqueous systems exhibits features analogous to those reported for other materials: the critical velocity decreases with increasing particle diameter, with the functional dependence suggesting that the interface remains planar behind the particle. The effects of solute concentration and thermal gradients indicate that the theoretical models determining critical velocities might have to be extended to transient conditions and coupled heat and mass diffusion. It might also be necessary to include interface stability criteria: the repulsion or entrapment of particles seems to be affected by the mechanisms controlling the transition between different morphologies of the solid-liquid interface, i.e. temperature and concentration distributions in combination with capillarity effects. For a clarification of these questions, specific experiments would be needed which extend the range of conditions analyzed so far, particularly with respect to thermal gradients, solute content as well as particle sizes and materials.

As a next step, similar experiments are performed to study the pushing and entrapment of biological cells [36]. Such observations can then be correlated with results obtained for particles under the same experimental circumstances. In this respect it would be of additional interest to investigate the interaction of particles and cells with a non-planar solidification front as it frequently occurs in many freezing situations. Such studies would be particularly relevant to cases where the particle or cell diameter considerably exceeds the spacing of the cellular or dendritic solidification structures. As pointed out in the beginning, it is important to determine the conditions under which biological cells get repelled or encapsulated, as their osmotic environment and the resulting de-

hydration are totally different in both cases [37]. The critical velocity is hence crucial with respect to osmotic damage and accordingly plays a significant role for successful cryopreservation.

Acknowledgements

The support of this study by the Max Kade Foundation, Inc., New York, NY, is gratefully acknowledged. The authors would also like to thank Shiva Ayyadurai and Jürgen Buschmann for their skillful assistance.

Symbols

a_0	Average intermolecular distance
B	Cooling rate
d	Distance between particle and interface
F	Force
G	Thermal gradient
k	Distribution coefficient
k'	Proportionality factor in eq. (6)
k''	Proportionality factor in eq. (7)
m	Exponent in eq. (7)
n	Exponent in eq. (6)
r	Particle radius
R	Radius of interface curvature
t	Time
T	Temperature
v	Velocity
x	Space coordinate
γ	Thermal coefficient
Δ	Difference
η	Viscosity
λ	Thermal conductivity
δ	Radial coordinate
ξ	Interface position
σ	Surface free energy

Indices

c	Critical
Cu	Copper
l	Liquid
p	Particle

R Edge of observation slit
s Solid

References

- [1] V.L. Bronstein, *J. Crystal Growth* 52 (1981) 345.
- [2] W.E. Brower, M.J. Freund, M.D. Baudino and C. Ringwald, *Cryobiology* 18 (1981) 277.
- [3] C. Körber, K. Wollhöver and M.W. Scheiwe, *Intern. J. Heat Mass Transfer* 26 (1983) 1241.
- [4] J.E. Lovelock, *Biochim. Biophys. Acta* 10 (1953) 414.
- [5] P. Mazur, *Fed. Proc.* 24 (1965) 175.
- [6] K.-H. Chen and W.R. Wilcox, *J. Crystal Growth* 40 (1977) 214.
- [7] A.W. Neumann, J. Szekely and E.J. Rabenda, *J. Colloid Interface Sci.* 43 (1973) 727.
- [8] S.N. Omenyi and A.W. Neumann, *J. Appl. Phys.* 47 (1976) 3956.
- [9] D.R. Uhlmann, B. Chalmers and K.A. Jackson, *J. Appl. Phys.* 35 (1964) 2986.
- [10] J. Cissé, and G.F. Bolling, *J. Crystal Growth* 10 (1971) 67.
- [11] P. Hoekstra and R.D. Miller, *J. Colloid Interface Sci.* 25 (1967) 166.
- [12] P. Aubourg, *Interaction of Second-Phase Particles with a Crystal Growing from the Melt*, PhD Thesis, MIT, Cambridge, MA (1978).
- [13] A.A. Chernov and V.L. Bronstein, *Soviet Phys.-Cryst.* 23 (1978) 4.
- [14] A.A. Chernov, D.E. Temkin and A.M. Melnikova, *Soviet Phys.-Cryst.* 22 (1977) 656.
- [15] D.E. Temkin, A.A. Chernov and A.M. Melnikova, *Soviet Phys.-Cryst.* 23 (1977) 13.
- [16] D. Langbein, *Fremdteilchen von einer Erstarrungsfront*, BMFT Bericht 01 QV 042-AK/SN (1983).
- [17] G.F. Bolling and J. Cissé, *J. Crystal Growth* 10 (1971) 56.
- [18] A.A. Chernov, D.E. Temkin and A.M. Melnikova, *Soviet Phys.-Cryst.* 21 (1976) 369.
- [19] D. Langbein, in: *Intermolecular Forces*, Ed. B. Pullmann (Reidel, Dordrecht, 1981).
- [20] J. Pötschke, in: *Spacelab-Nutzung, Status-Seminar des BMFT, DFVLR-Bericht 80-02* (1981).
- [21] J. Pötschke, *Wechselwirkung der Erstarrungsfront mit Fremdphasenteilchen Proceedings, Workshop Erstarrungsfrontdynamik* (Giesserei-Institut, RWTH, Aachen, 1981).
- [22] G. Carrier, personal communication, cited by Uhlmann et al. [9].
- [23] E.J. Workman and S.E. Reynolds, *Phys. Rev.* 78 (1950) 254.
- [24] G.W. Gross, *Advan. Chem. Ser.* 73 (1968) 27.
- [25] I.D. Harrison and W.A. Tiller, in: *Ice and Snow*, Ed. W.D. Kingery (MIT Press, Cambridge, MA, 1963).
- [26] C. Körber, M.W. Scheiwe and K. Wollhöver, *Cryobiology* 21 (1985) 68.
- [27] C. Körber, K. Wollhöver and M.W. Scheiwe, *J. Crystal Growth* 61 (1983) 307.

- [28] M.D. Cosman, Effects of Cooling Rate and Supercooling on the Formation of Ice in a Cell Population, PhD Thesis, MIT, Cambridge, MA (1983).
- [29] M.W. Scheiwe and C. Körber, *J. Microscopy* 126 (1982) 29.
- [30] M.W. Scheiwe and G. Rau, *Chem.-Ing.-Tech.* 53 (1981) 787.
- [31] J. Buschmann, Untersuchung wandernder Phasengrenzflächen in wässrigen Lösungen und Suspensionen, Diplom-Thesis, RWTH Aachen (1983).
- [32] K. Wollhöver, Ch. Körber, M.W. Scheiwe and U. Hartmann, *Intern. J. Heat Mass Transfer* 28 (1985) 761.
- [33] K. Wollhöver, M.W. Scheiwe, U. Hartmann and Ch. Körber, *Intern. J. Heat Mass Transfer*, in press.
- [34] W.W. Mullins and R.F. Sekerka, *J. Appl. Phys.* 35 (1964) 444.
- [35] J.S. Langer, *Rev. Mod. Phys.* 52 (1980) 1.
- [36] C. Körber, G. Rau, M.D. Cosman and E.G. Cravalho, *Cryo-Letters*, in preparation
- [37] K. Wollhöver, M.W. Scheiwe and Ch. Körber, *Cryobiology* 20 (1983) 736.